High-Sensitivity Electron Paramagnetic Resonance of Mn_{12}-Acetate

S. Hill*
Department of Physics, Montana State University, Bozeman, Montana 59717

J. A. A. J. Perenboom
Research Institute for Materials and High Field Magnet Laboratory, University of Nijmegen, 6525 ED, The Netherlands

N. S. Dalal and T. Hathaway
Chemistry Department and National High Magnetic Field Laboratory, Florida State University, Tallahassee, Florida 32310

T. Stalcup and J. S. Brooks
Department of Physics and National High Magnetic Field Laboratory, Florida State University, Tallahassee, Florida 32310
(Received 4 August 1997)

The energy diagram of Mn_{12}-acetate is probed close to the top of the anisotropy barrier using a novel, high-sensitivity, electron paramagnetic resonance technique. Multiple resonances, and their temperature dependence, are observed from 35 to 115 GHz, for a single high-quality crystal. The data are sufficiently detailed to make extremely accurate comparisons with predictions based on a spin $S = 10$ Hamiltonian. Although overall agreement is good, we find evidence for possible inadequacies of this model. [S0031-9007(98)05531-8]

PACS numbers: 75.45.+j, 36.40.Cg, 76.30.–v

The Mn_{12} cluster complex [1], $[Mn_{12}O_{12}(CH_3COO)_{16}(H_2O)_4] \cdot 2CH_3COOH \cdot 4H_2O$ (Mn_{12}-Ac), has attracted considerable interest due to indications that it exhibits the phenomenon of macroscopic quantum tunneling of magnetic moment (QTM) [2]. The core of the Mn_{12}-Ac cluster consists of a tetrahedron of four Mn(IV) ions, each with $S = 3/2$, surrounded by eight Mn(III) ions with $S = 2$. The clusters crystallize into a tetragonal lattice in which the angular momentum is thought to be completely quenched, and a Jahn-Teller distortion gives rise to a strong axial anisotropy [1]. Superexchange leads to a high spin ground state where the spins of the Mn(IV) and Mn(III) ions are coupled parallel to $S = 6$ and $S = 16$, respectively; the spins of the outer shell are directed antiparallel to the spins of the inner ions. In the ground state, therefore, the cluster may be treated as an $S = 10$ object, with the spin preferentially aligned along the **c** axis due to the axial anisotropy [3,4].

Magnetization studies have confirmed the $S = 10$ character of Mn_{12}-Ac [4]. In addition, high-field electron paramagnetic resonance (EPR) studies on powders and polycrystalline samples have provided considerable information concerning the spin Hamiltonian of the system [3–5]. Nevertheless, the precise nature of the relaxation of the magnetization at low temperatures remains unclear.

To lowest order, the spin Hamiltonian may be written $H = D_1 S_z^2 - g\mu_B \mathbf{B} \cdot \mathbf{S}$ [6]. Thus, pairs of $\pm M_S$ levels are degenerate in zero magnetic field, where M_S is the projection of S along the sample's easy (**c**, or z) axis. The anisotropy constant D_1 is known to be negative so that the $M_S = \pm 10$ levels lie lowest in energy, while the $M_S = 0$ level lies highest. When the system is spin polarized by applying and removing a large magnetic field ($g\mu_B \mathbf{B} > S \times D_1$) parallel to the sample's easy axis, a sizeable energy barrier inhibits the reversal of this moment; the magnitude of this barrier is $\sim 10^2 \times D_1 \approx 44.5$ cm^{-1} [7]. In spite of this, considerable experimental evidence suggests that the spin system is somehow able to overcome this barrier at low temperatures [8]. Below about 3 K, steps are observed in the hysteresis loop of oriented powder samples [9,10] and single crystals [11]. The occurrence of these steps, at more-or-less regularly spaced values of magnetic field, has been cited as evidence that the magnetization reversal is due to QTM [2]. Unlike superparamagnetic particles, where QTM was first observed [2], Mn_{12}-Ac contains a large number of identical spin clusters, allowing much more accurate comparisons with theory to be made.

Until now, no single crystal EPR studies of Mn_{12}-Ac have been possible. In this investigation, we utilize a somewhat novel approach—a multifrequency, high-sensitivity EPR technique that enables us to make measurements on submillimeter sized single crystals. This is made possible by the use of resonant cavities with resonance frequencies varying from 35 to 115 GHz. This frequency range allows us to probe the energy levels immediately below the top of the anisotropy barrier which, as recent ac susceptibility measurements have indicated, may be crucial to the magnetization relaxation mechanism [12]. Furthermore, EPR transitions between these levels occur in the 0–5 T range (see below), precisely the region where the magnetization steps are seen.

The high sensitivity of our method is a result of high cavity Q factors ranging from 5×10^3 to 2×10^4, representing an improvement in sensitivity by at least 3 orders of magnitude relative to conventional high-field EPR

techniques [3–5]. This sensitivity enhancement is crucial to the successful measurement of single crystals, since the submillimeter sizes of the best available samples make it impossible for resonances to be detected by single-pass EPR techniques. Finally, our technique does not require narrow-band magnetic field modulation for detecting the resonances. This is a definite advantage in our case, where the resonance lines are broad (a few hundred mT).

The Mn_{12}-Ac crystals were synthesized following the original procedure described by Lis [1], and grew in the form of rectangular parallelepipeds with the **c** axis as the longest dimension (direction of easy magnetization); the sample dimensions were $\approx 1 \times 0.3 \times 0.3$ mm^3. The sample authenticity was confirmed by dc magnetization measurements which exhibited the expected magnetization steps below 3 K [13,14].

Slightly oversized cylindrical copper cavities were used in transmission, providing several modes in the desired frequency range [15]; predominantly TE01p ($p = 1, 2, \ldots$) modes were excited. A single Mn_{12}-Ac crystal was placed close to the bottom of the cavity, halfway between its axis and its perimeter, thereby ensuring that the sample was optimally coupled to the radial ac magnetic fields ($\mathbf{B}_1$) for a given TE01p mode. The applied dc magnetic field ($\mathbf{B}_0$) was directed parallel to the cavity axis, so that $\mathbf{B}_1$ was perpendicular to $\mathbf{B}_0$ for all of the measurements. The sample was then loaded in three configurations, corresponding to the dc magnetic field ($\mathbf{B}_0$) being applied parallel to each of the sample's **a**, **b**, and **c** axes. The cavity and, therefore, the sample could accurately and controllably be maintained at any temperature in the range from 1.25 to 60 K. Both superconducting and resistive magnets were employed. As a source and detector, we utilized a Millimeter-Wave Vector Network Analyzer (MVNA) [15,16].

Figure 1(a) shows the temperature dependence of the transmission through the cavity for a single frequency, $\nu = 66.135$ GHz (~ 2.2 cm^{-1}), with $\mathbf{B}_0 \parallel \mathbf{c}$. The sharp minima correspond to absorption in the sample due to EPR; complementary data were obtained for the dispersion. A strong feature is observed at ~ 2.5 T (labeled **X**), which broadens on cooling. From the frequency dependence of **X**, we have established that it has negligible zero-field offset and, therefore, cannot be reconciled with the energy diagram in Fig. 1(b) (see below). Furthermore, the temperature dependence of **X** is very different from the other features in Fig. 1(a). Consequently, we conclude that **X** is due to isolated impurities in the sample (possibly Mn^{2+}); no resonant features are observed in the empty cavity.

The complexity of the EPR spectra in Fig. 1(a) increases as the temperature is raised, i.e., new resonances develop on the low-field side of **X**. This temperature dependence is consistent with the thermal population of levels close to the top of the barrier. Figure 1(b) shows the results of a recent calculation of these levels which was motivated primarily by magnetization measurements [13]. In order to maintain consistency between this calculation, and available experimental data (our own [13], as well as other published

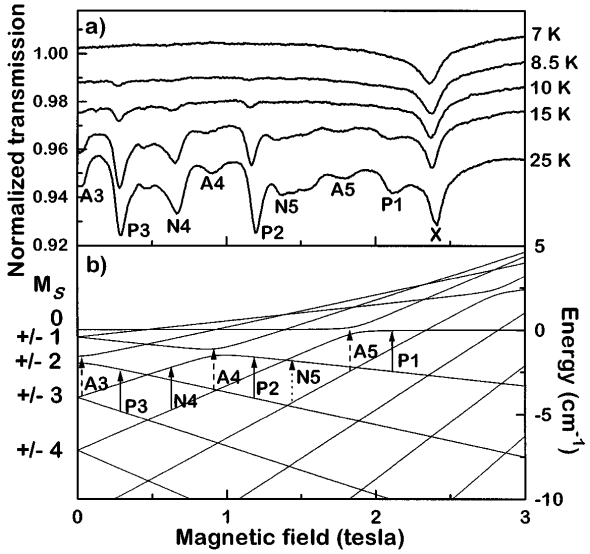

FIG. 1. (a) Temperature dependence of the normalized transmission (offset) for $\mathbf{B}_0 \parallel \mathbf{c}$; the frequency is 66.135 GHz. (b) A calculation of the corresponding energy levels for the $S = 10$ spin system [13]; the arrows indicate transitions responsible for the resonances in (a). See text for details of the calculation and for an explanation of the labels.

results [9–11]), higher order terms in the spin Hamiltonian were considered, e.g., $D_{4\parallel} \times S_z^4 + D_{4\perp} \times (S_x^4 + S_y^4)$ [17]. Such fourth order terms have been discussed previously in connection with QTM [5,6], and are responsible for the observed anticrossings between levels with $\Delta M_S = \pm 4$ [see Fig. 1(b)]. A more detailed justification for considering such higher order terms may be found in Ref. [13]. Nevertheless, we wish to emphasize that the parameters used in obtaining the level diagram in Fig. 1(b) were additionally constrained by the EPR data presented here (see below).

We are now in a position to assign the transitions depicted in Fig. 1(b) to the resonances observed in Fig. 1(a). It can be seen that, for each pair of zero-field levels ($\pm M_S$), two series of resonances are observed, one corresponding to transitions between levels aligned with the field ($+M_S$) and the other to transitions between levels which are antialigned ($-M_S$). Several of the resonances in Fig. 1(a) have been labeled **P** ($+M_S$) or **N** ($-M_S$) to distinguish between these cases. Additional resonances are observed for this, and other frequencies, which we label **A**. The numbering after the letters **P**, **N**, or **A** denotes the value of M_S for the level from which the transition was excited. It is found that the **A** resonances are observed only over narrow intervals in magnetic field in the general vicinity of the anticrossings seen in Fig. 1(b) (0.9 T, 1.8 T, etc.). It is, therefore, tempting to attribute the **A** resonances to these anticrossings, thereby providing direct evidence supporting the level diagram in Fig. 1(b). However, we cannot rule out other possibilities.

It is to be noted that the relative intensities of the resonances in Fig. 1(a) are qualitatively consistent with a thermal population of these high-lying (low M_S) levels,

i.e., the **P3** and **N4** transitions are strongest because they are excited from the lowest-lying levels.

The frequency dependence of the data for $\mathbf{B}_0 \parallel \mathbf{c}$ is shown in Fig. 2; all of the data points fall on one of several straight lines. The solid points fall on a line through the origin and correspond to the impurity resonance (**X**). The remaining points lie on straight lines with finite zero-field offsets. For each offset, two series of resonances are observed, corresponding to the **P** (positive slope) and **N** (negative slope) transitions. It should be noted that the fields where the **P** and **N** data cross (0.45 T, 0.9 T, 1.35 T, etc.) coincide with the fields where magnetization steps are observed below 3 K [9–11,13].

The zero-field offsets measured here (Fig. 2), and those obtained previously by Caneschi *et al.* [4] contain key information concerning the nature of the spin Hamiltonian. As discussed above, attempts to simulate the present data are vastly improved if a considerable fourth order term is taken into consideration in the Hamiltonian [13]. This is best illustrated by noting that the zero-field offsets in Fig. 2 do not occur in the simple ratio 1:3:5:7:etc., as expected in the absence of a fourth order term. The *best* correspondence between the data and the calculation is obtained assuming $D_1 = -0.47$ cm^{-1} and $D_{4\perp} = -3.5 \times 10^{-4}$ cm^{-1} ($= D_{4\parallel}$) [17]. However, noticeable deviations are unavoidable for the one or two levels closest to the top of the barrier. This indicates possible evidence for a breakdown of the assumption that the Mn_{12} clusters may be treated strictly as rigid $S = 10$ objects. The value obtained for D_1 ($= -0.47$ cm^{-1}) is slightly larger than the generally accepted value corresponding to the barrier height of 44.5 cm^{-1} ($= 10^2 \times D_1$) [7]. However, it has been noted that magnetization relaxation probably occurs via levels below the top of the barrier [12], thus reducing its apparent height to some degree.

From straight line fits to the different sets of **P** data in Fig. 2, g values varying between 1.97 (largest offset) and 2.08 (smallest offset) are obtained. Once again, these findings clearly identify possible inadequacies of the $S = 10$ Hamiltonian. The g value used in our calculation of Fig. 2(b) is $g_\parallel = 2.05$, which is rather larger than the published value of 1.9 [3,4].

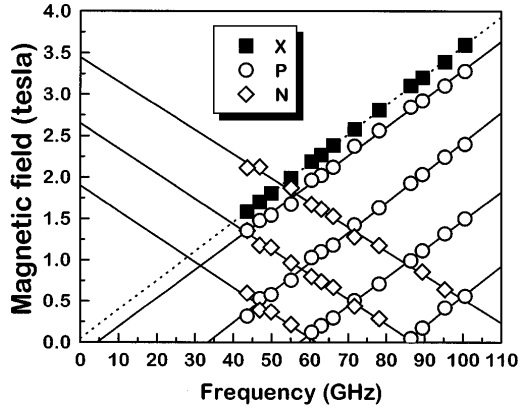

FIG. 2. Frequency dependence of the data for $\mathbf{B}_0 \parallel \mathbf{c}$.

Although the frequencies used here are smaller than the largest zero-field splittings (~9 cm^{-1} for the largest M_S), we have clearly been able to obtain a considerable amount of information concerning the levels close to the barrier. The nature of the energy level diagram for $\mathbf{B}_0 \perp \mathbf{c}$ allows us to probe the entire structure of the system. This is visualized in Fig. 3(b), where it can be seen that the field causes a strong coupling, and eventual anticrossing, of levels separated at zero field by $\Delta M_S = \pm 1$. This results in a lifting of the degeneracy between the $\pm M_S$ levels and, because of level mixing, the possibility of a multitude of transitions between the levels in Fig. 3(b).

Figure 3(a) shows EPR spectra obtained at several temperatures for $\mathbf{B}_0 \perp \mathbf{c}$; the frequency is 111.119 GHz (~3.7 cm^{-1}). As pointed out above, a complex EPR spectrum is observed for this geometry. At high fields (>4 T), however, two distinct series of resonances are discernible—this is seen most clearly for the 20 K data, where the intensity alternates between the resonances which are labeled α and β. In contrast to the data in Fig. 1(a), most of the resonances are observed at fields above the impurity feature (labeled **X**). Thus, the data in Figs. 1(a) and 3(a) confirm the high degree of axial anisotropy. It is to be noted that many of the features in Fig. 3(a), observed at fields below **X**, occur in the same field range as the resonances seen for $\mathbf{B} \parallel \mathbf{c}$ (see Fig. 2). Thus, it would be impossible to distinguish between these resonances from measurements on polycrystalline or powder samples.

The resonances labeled α persist to the lowest frequencies used in this investigation (see Fig. 4 below), while the remaining resonances are observed only at higher frequencies. From these facts, we are able to assign the α resonances to transitions between the split doublets ($\pm M_S$

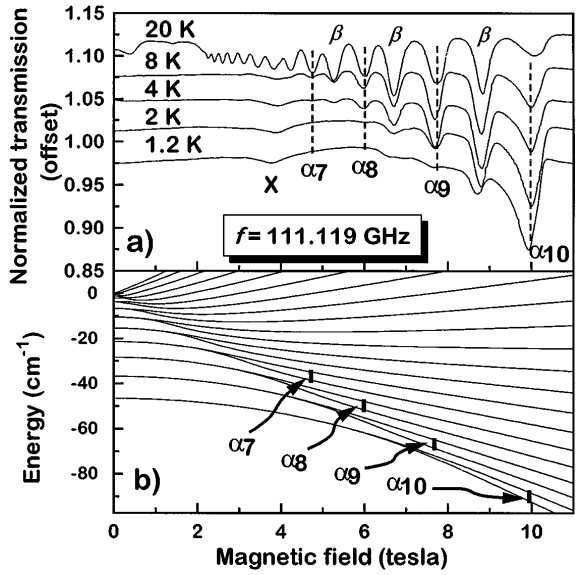

FIG. 3. (a) EPR spectra obtained at several temperatures, for $\mathbf{B}_0 \perp \mathbf{c}$ (see text for explanation of labels). (b) A calculation of the corresponding energy levels [13]; the arrows indicate the transitions responsible for the resonances in (a).

in zero field), as indicated in Fig. 3(b); these transitions are allowed only because of the strong level mixing. On the basis of the positions of the α resonances, and their frequency dependence, we have been able to simulate the data for this orientation using the same D values as above. However, in this case, the published value of $g_\perp = 1.9$ (Caneschi *et al.* [4]) is in good agreement with our data, implying an anisotropic g value. Independent measurements with $\mathbf{B}_0 \parallel \mathbf{a}$, and $\mathbf{B}_0 \parallel \mathbf{b}$, rule out any orthorhombic distortions of the crystal symmetry down to 5 K.

The origin of the resonances labeled β is not as straightforward. At intermediate fields ($\sim$1–10 T), such that the Zeeman energy is comparable to the zero-field level spacings $[g\mu_B\mathbf{B} \sim (2M_S - 1) \times 0.47 = (0.5\text{–}9\ \mathrm{cm}^{-1})]$, the levels are strongly mixed, as noted above. Therefore, transitions are allowed between the levels in adjacent doublets, i.e., levels having $\pm M_S$ and $\pm(M_S \pm 1)$ in zero field. However, a threshold energy exists for such transitions, corresponding to the minimum energy separation (at the point of closest approach) of the levels in question. This accounts for the disappearance of the β resonances at lower frequencies, and the rich EPR spectra observed at higher frequencies, e.g., as seen in Fig. 3(a).

Finally, Fig. 4 shows magnifications of intermediate frequency data obtained for each orientation, i.e., $\mathbf{B}_0 \perp \mathbf{c}$ (main part of Fig. 4), and $\mathbf{B}_0 \parallel \mathbf{c}$ (inset). The first point to note is the disappearance of most of the β resonances for $\mathbf{B}_0 \perp \mathbf{c}$ at this lower frequency of 57.4 GHz [see also Fig. 3(a)]. However, more significant is the increase in intensity, with decreasing temperature, of the features labeled γ. In fact, the temperature dependence of γ, in the main part of Fig. 4, is qualitatively similar to the temperature dependence of $\alpha\mathbf{10}$, the fundamental resonance excited from the ground state, i.e., these are the only resonances which diminish in intensity as the temperature is raised. This suggests that, like the $\alpha\mathbf{10}$ transition, a finite population of spins exists at low temperatures from which the γ transitions are excited. This is particularly significant for the $\mathbf{B}_0 \parallel \mathbf{c}$ data, since only transitions between levels close to the top of the barrier are accessible with these frequencies, thus suggesting that there may be a metastable (or dynamic equilibrium) population of spins close to the barrier, even at $T = 0$ K. It is not clear whether the γ transitions can be explained within the framework of an $S = 10$ spin system; however, they are definitely due to the sample.

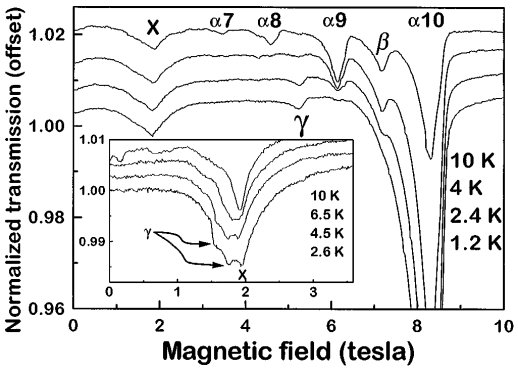

FIG. 4. Magnifications of intermediate frequency EPR data obtained for each orientation; for $\mathbf{B}_0 \perp \mathbf{c}$ (main part of figure), the frequency is 57.4 GHz; and for $\mathbf{B}_0 \parallel \mathbf{c}$ (inset), the frequency is 55.16 GHz. The temperatures are indicated in the figures. Also, see text for explanation of labeling.

In conclusion, we have used a high-sensitivity EPR technique to make an extremely detailed investigation of the energy level diagram of Mn_{12}-Ac close to the top of the magnetization reversal barrier. The ability to study single crystals is a distinct advantage in that it allows us to observe multiple resonances, and their temperature dependence, with the magnetic field applied at any orientation with respect to the sample; we argue that this study would not have been possible using powder or polycrystalline samples. At first sight, our data appear to agree well with the behavior expected of an $S = 10$ spin system. Furthermore, we see possible evidence supporting recent calculations in which higher(fourth)-order terms in the spin Hamiltonian are included [13]. However, agreement is not quite as good for EPR transitions close to the top of the anisotropy barrier, suggesting possible inadequacies of the $S = 10$ Hamiltonian. From temperature dependent studies (down to 1.2 K), we find compelling evidence suggesting that a small population of spins may exist close to the top of the anisotropy barrier, even at low temperatures.

This work was supported under NSF-DMR 95-10427 and by the National High Magnetic Field Laboratory.

*Electronic address: hill@physics.montana.edu

[1] T. Lis, Acta Crystallogr. Sect. **36**, 2042 (1980).
[2] For a review, see *Quantum Tunneling of Magnetization—QTM'94*, edited by L. Gunther and B. Barbara, NATO ASI Ser. E, Vol. 301 (Kluwer, Dordrecht, 1995).
[3] R. Sessoli *et al.*, J. Am. Chem. Soc. **115**, 1804 (1993).
[4] A. Caneschi *et al.*, J. Am. Chem. Soc. **113**, 5873 (1991).
[5] A. L. Barra *et al.*, Phys. Rev. B **56**, 8192 (1997).
[6] P. Politi *et al.*, Phys. Rev. Lett. **75**, 537 (1995).
[7] M. A. Novak *et al.*, J. Magn. Magn. Mater. **146**, 211 (1995).
[8] R. Sessoli *et al.*, Nature (London) **365**, 141 (1993).
[9] J. R. Friedman *et al.*, Phys. Rev. Lett. **76**, 3830 (1996).
[10] J. M. Hernandez *et al.*, Phys. Rev. B **55**, 5858 (1997).
[11] L. Thomas *et al.*, Nature (London) **383**, 145 (1996).
[12] F. Luis *et al.*, Phys. Rev. B **55**, 11 448 (1997).
[13] J. A. A. J. Perenboom *et al.*, (to be published).
[14] These steps were also observed in the microwave experiment [S. Hill (unpublished)].
[15] S. Hill *et al.*, in *Millimeter and Submillimeter Waves III*, edited by Mohammed N. Afsar (The International Society for Optical Engineering, Bellingham, 1996), p. 296.
[16] Manufactured by AB*mm*, 52 Rue Lhomond, 75005 Paris, France.
[17] This unconventional notation is used to maintain consistency with Ref. [13]. The $D_{4\parallel}$ and $D_{4\perp}$ parameters may be related to the more widely used B_4^0 and B_4^4 parameters as follows: $B_4^4 = \frac{1}{4}D_{4\perp}$; $B_4^0 = \frac{1}{20}\{\frac{3}{7}D_{4\perp} + \frac{4}{7}D_{4\parallel}\}$.